



RESEARCH ARTICLE

A CFD SIMULATION OF WATER FLOW THROUGH A VARIABLE AREA VENTURI METER

*Akpan, Patrick Udeme-obong

Department of Mechanical Engineering, University of Nigeria, Nsukka

ARTICLE INFO

Article History:

Received 05th December, 2013
Received in revised form
10th January, 2014
Accepted 14th February, 2014
Published online 25th March, 2014

Key words:

CFD Simulation,
k- Turbulence model,
Ansys Fluent,
Venturi meter,
Water flow.

ABSTRACT

This work Investigates using the Ansys fluent CFD tool, the pressure difference exerted on a bluff body object and discusses the flow field from inlet to outlet. The objectives of this work are to discuss the flow field from inlet to outlet, to investigate the pressure difference exerted 25mm upstream and 25mm downstream of the bluff body object for different volumetric flow rates (4 l/s, 5 l/s and 8 l/s). The total pressure losses across the plate for the 4 l/s, 5 l/s and 8 l/s flows are 17.38 kPa, 27.14 kPa and 69.62 kPa respectively. These losses are partly due to the level of turbulence with the 8 l/s flow having the maximum turbulence intensity of over 250% exceeding those of the 4l/s and 5l/s flows which are ~130% and ~160% respectively. When compared with the mean operating pressure (101.325 kPa), these pressure losses represents 17.1%, 26.8% and 68.7% change for 4l/s 5 l/s and 8 l/s flows respectively.

Copyright © 2014 Akpan, Patrick. This is an open access article distributed under the Creative Commons Attribution License, which permits unrestricted use, distribution, and reproduction in any medium, provided the original work is properly cited.

INTRODUCTION

Computational Fluid Dynamics (CFD) is an aspect of fluid mechanics that utilizes numerical methods and algorithms to solve and analyze fluid flow problems (Blazek 2001; Chung 2002). The governing sets of equations which are solved include the continuity equations, Navier-Stokes equations and any additional conservation equations like energy and species concentrations. Computers are used to perform calculations required to simulate the interaction of fluids with surfaces defined by boundary conditions. A venturi meter is used to measure the volumetric flow rate (\dot{V}) of a fluid by making use of the venturi effect (the reduction of fluid pressure that results when fluid flows through a constricted section of pipe) (Philip *et al.*, 2012; Morris 2001). It could also be used for mixing a liquid with a gas. This venturi effect is an outcome of applying the Bernoulli's equation (Eq. 1) to an ideal incompressible fluid flow along a conduit surface with varying cross sectional area (see Figure.1).

$$\frac{P}{\rho} + \frac{1}{2}u^2 + gz = Constant \tag{1}$$

But since z is approximately constant for the two sections (1) and (2) in Figure 1, therefore Eq. 1 becomes

*Corresponding author: Akpan, Patrick,
Department of Mechanical Engineering, University of Nigeria,
Nsukka.

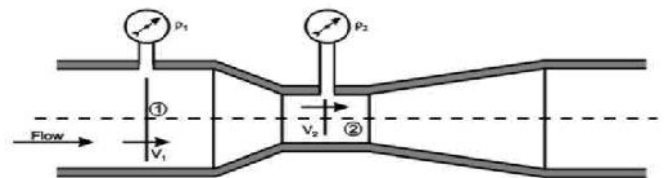


Figure 1. A cross-sectional view of a typical venturi

$$P + \frac{1}{2}\rho u^2 = P_0 \tag{2}$$

Where P_0 is the total pressure made up of the static (P) and dynamic ($\frac{1}{2}\rho u^2$) pressures. Applying the continuity equation across section (1) and (2);

$$\dot{V} = u_1 A_1 = u_2 A_2 \tag{3}$$

And combining equations (2) and (3) we get the volumetric flow rate (see Eq. 4) at any section along the flow for an ideal flow expressed as a function of the pressure drop across the constriction lying between sections (1) and (2) along the flow.

$$\dot{V} = A_1 \sqrt{\frac{2(P_1 - P_2)}{\rho \left(\left(\frac{A_1}{A_2}\right)^2 - 1 \right)}} = A_2 \sqrt{\frac{2(P_1 - P_2)}{\rho \left(1 - \left(\frac{A_1}{A_2}\right)^2 \right)}} \tag{4}$$

Estimation of Permanent Pressure Loss for the flow through Obstruction type flow meters helps the selection of flow meter

for industrial applications if the operating pressure is known. Experimental determination of permanent pressure loss is both time consuming and expensive (Durst and Wang 1989; Prajapati *et al.* 2010). This work is a numerical experimentation done to simulate and analyze water flow through a variable area venturi meter using a commercial computational fluid dynamics (CFD) package FLUENT. The objectives of this task are: To discuss the flow field from inlet to outlet, To investigate the pressure difference exerted 25mm upstream and 25mm downstream a bluff body object for different volumetric flow rates (4 l/s, 5 l/s and 8 l/s) and to compare the pressure difference determined from a course and fine mesh.

MATERIALS AND METHODS

Pre-Processing

Geometric Model and Meshing

The geometric model of the venturi meter that was modeled is shown in Figure 2. The mesh size information for both course and fine are given on Table 1. The sizes of the mesh around the bluff body were made so small around the bluff body to capture adequately the physics of the flow problem.

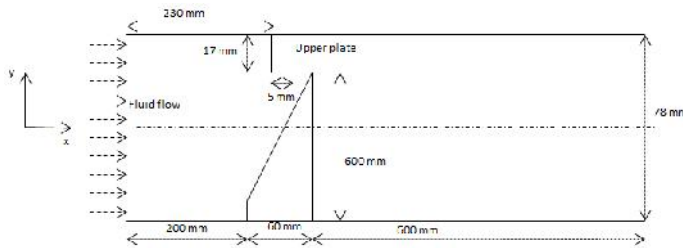


Figure 2. The geometric model

Table 1. Mesh size information of course and fine mesh

Mesh Type	Level	Cells	Faces	Nodes	Partitions	Cell Zone	Face Zone
Course	0	13580	25542	11963	1	1	5
Fine	0	54118	101121	47004	1	1	5

Inlet velocity, Reynolds number and Turbulence Intensity calculation

From the flow parameters given, the inlet area, velocities, Reynolds numbers were calculated. The turbulence intensity (I) was using Eq. 5. The turbulence intensity calculated for the 4 l/s, 5 l/s and 8 l/s flows are 3.285 %, 3.182 % and 2.976 % respectively. These are medium inlet turbulent intensity cases (Fluent Inc. 2006a).

Flow Parameters Given:

Volumetric flow rates (\dot{V}) = 4 l/s, 5 l/s and 8 l/s

Pipe diameter (D) = 0.078 m

Density of water (ρ) = 998.2 kg/m³

Dynamic viscosity of water (μ) = 0.001003 kg/ms

$$I = 0.16 \times \left(\frac{\rho u D}{\mu} \right)^{-1} \quad (5)$$

Processing (Solver Execution)

In setting up the simulation, The Ansys fluent 12.1 version was launched in 2D, double precision mode. And the mesh was checked for errors. As soon as this was done, these procedures were followed:

Solver Properties and Viscous model Selection

Pressure based solver was selected. In this approach, the pressure field is extracted by solving a pressure or pressure correction equation which is obtained by manipulating the continuity and momentum equations. *Steady state and absolute velocity formulation* were also selected. Since a viscous incompressible flow was considered, with some turbulence intensity, the *k-ε Turbulence model* based on the eddy viscosity hypothesis was selected to model the fluid flow. The decision to use this turbulence model is that it is reasonably accurate and economic in computational cost (Fluent Inc. 2006b). The solution of two additional equations by this model for the turbulent kinetic energy (TKE) and turbulent dissipation rate (TDR) (ϵ) in Eqs. 6 and 7 respectively is used to determine the turbulent eddy viscosity (ν_T) in Eq. 8 which is related to the Reynolds stresses ($\overline{u_i u_j}$) in Eq. 9.

$$\frac{\partial k}{\partial t} + \bar{u}_j \frac{\partial k}{\partial x_j} = \frac{\partial}{\partial x_j} \left[\left(\frac{\nu_T}{\sigma_k} + \nu \right) \frac{\partial k}{\partial x_j} \right] + \nu_T \left(\frac{\partial \bar{u}_j}{\partial x_i} + \frac{\partial \bar{u}_i}{\partial x_j} \right) \frac{\partial \bar{u}_i}{\partial x_j} - \epsilon \quad (6)$$

$$\frac{\partial \epsilon}{\partial t} + \bar{u}_j \frac{\partial \epsilon}{\partial x_j} = \frac{\partial}{\partial x_j} \left[\left(\frac{\nu_T}{\sigma_\epsilon} + \nu \right) \frac{\partial \epsilon}{\partial x_j} \right] + C_{\epsilon 1} \frac{\epsilon}{k} \nu_T \left(\frac{\partial \bar{u}_j}{\partial x_i} + \frac{\partial \bar{u}_i}{\partial x_j} \right) \frac{\partial \bar{u}_i}{\partial x_j} - C_{\epsilon 2} \frac{\epsilon^2}{k} \quad (7)$$

$$\nu_T = C_\mu \frac{k^2}{\epsilon} \quad (8)$$

$$\overline{u_i u_j} - \frac{2}{3} k \delta_{ij} = -\nu_T \left(\frac{\partial \bar{u}_j}{\partial x_i} + \frac{\partial \bar{u}_i}{\partial x_j} \right) \quad (9)$$

Once the Reynolds stresses are determined, they are used in the Reynolds Average Navier Stokes (RANS) equation (Eq. 10) in conjunction with the continuity equation (Eq. 11) to determine the fluid flow field.

$$\frac{\partial \bar{u}_i}{\partial t} + \bar{u}_j \frac{\partial \bar{u}_i}{\partial x_j} = -\frac{1}{\rho} \frac{\partial \bar{P}}{\partial x_i} + \frac{\partial}{\partial x_j} \left[\nu \left(\frac{\partial \bar{u}_j}{\partial x_i} + \frac{\partial \bar{u}_i}{\partial x_j} \right) \right] + F_i \frac{\partial \overline{(u_i u_j)}}{\partial x_j} \quad (10)$$

$$\frac{\partial \bar{u}_j}{\partial x_j} = 0 \quad (11)$$

Material, Boundary Conditions and Solution Specifications

Under the materials option, Liquid water was selected and copied from the fluent data base. Liquid water was also selected in the cell zone condition. The default atmospheric pressure of 101.325 kPa was used as the operating condition. The boundary conditions for the inflow were set based on the values of velocity, turbulence intensity and the hydraulic diameter of the pipe calculated while the outflow boundary condition was used as a pressure outlet boundary specified by using zero gauge pressure. Pressure velocity coupling was achieved by means of SIMPLE (Semi-Implicit Pressure linked equation proposed by Patankar and Spalding (1972)). For Spatial discretisation the order of discretisation used were;

gradient (Least square cells based), pressure (standard), momentum (Second order upwind), turbulent kinetic energy (second order upwind), turbulent dissipation rate (Second order upwind) The default under-relaxation factors were used: Pressure (0.3), density (1), body forces (1), momentum (0.7), and turbulent kinetic Energy (0.8), and turbulent dissipation rate (0.8), turbulent viscosity. These values are needed to stabilise the solution. The monitor check convergence criteria was set at 10^{-06} for the residuals of continuity, x-velocity, y-velocity, k and ϵ . The solution was initialised from the inlet with reference frame relative to the cell zone. The iteration was set at 4000 times for all the flow rates including the course mesh. This is this is to ensure that all the convergence criteria were satisfied.

RESULTS AND DISCUSSION (POST PROCESSING)

The solution for the simulations carried out for the 4 l/s, 5 l/s and 8 l/s flows converged after 3390, 3383 and 3395 iterations respectively. The coarse mesh case converged after 1415 iterations. Please note that only some selected plots representing the resulting flow field are discussed in sections 3.1 -3.5.

Streamlines

Figures 3, 4 and 5 represents the upstream, midstream and downstream streamlines for the 5 l/s case. The flow upstream (Fig. 3) is laminar as the stream lines are in a uniform straight line. At mid-stream (Fig. 4) where turbulence is experienced, it is evident that flow separation and recirculation caused by adverse pressure difference occurs. Two recirculation zones can be seen. As the flow continued downstream (Fig. 5), the dividing streamlines reattached to the walls of the Venturi and continued until it got to the end of the flow. This same pattern was observed from the 4 l/s and 8 l/s inlet flows.

maximum recirculation velocity for the 4 l/s, 5 l/s and 8 l/s flow rates are - 1.92 m/s, -2.3 m/s and -3.7m/s respectively. The negative sign implies that the flow direction is reverse in the recirculation zones.

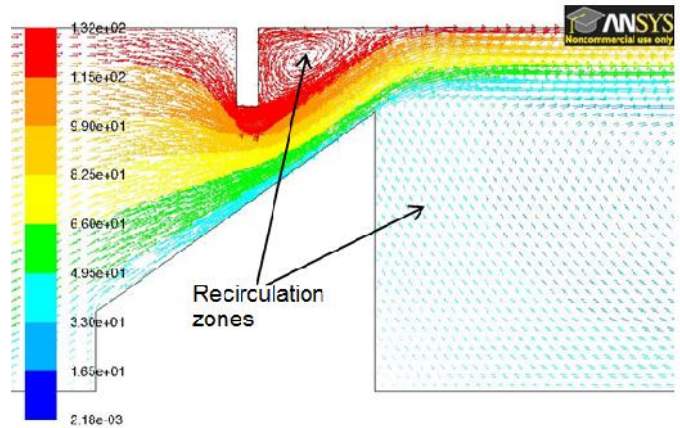


Figure 4. Mid-stream stream function for 5 l/s

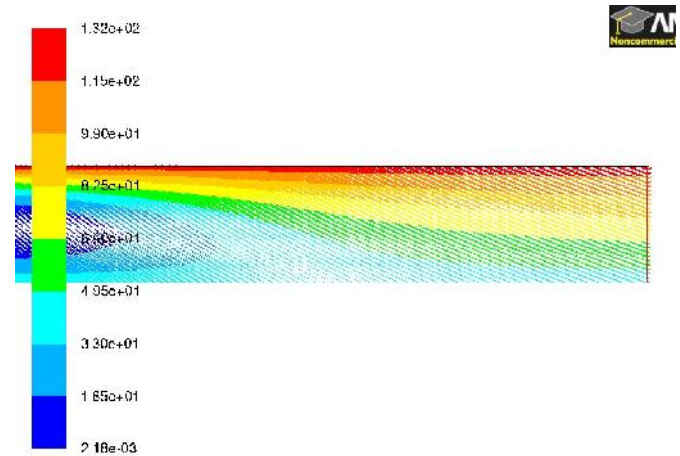


Figure 5. Downstream stream function for 5 l/s flow

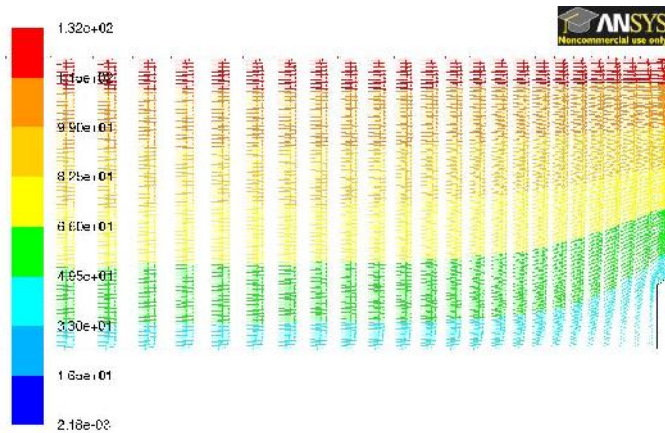


Figure 3. Upstream stream function for 5 l/s

Velocity contours and Vectors

The maximum velocity in the flow field is experienced downstream of the bluff body on the top wall surface (Fig. 6). The reduction in cross sectional area causes increase in velocity. This is also the case with the 4 l/s and 8 l/s flow rate. The maximum recirculation velocity increases in those recirculation zones with increase in volumetric flow rate. The

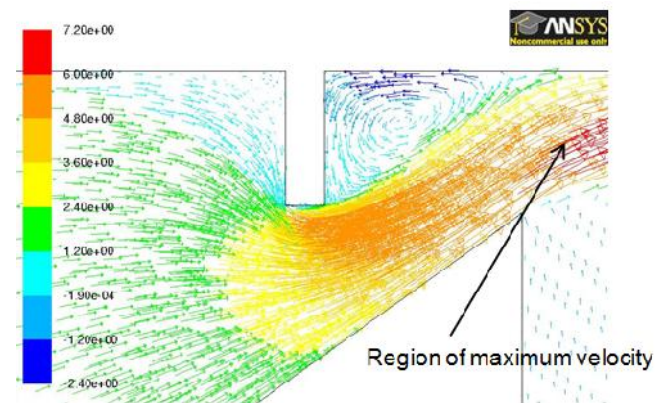


Figure 6. X-Velocity vector for the 5 l/s showing details of flow around the Plate

The flow fields take the same pattern irrespective of the flow velocity with an upstream total pressure that is largely static. Fig. 7 represents the pressure contour for the 5 l/s flow. The maximum total pressure increased with increase in volumetric flow rate in the flow field. This is in accordance with the Bernoulli's relation as dynamic pressure effects are chiefly responsible for this.

Pressure Contours

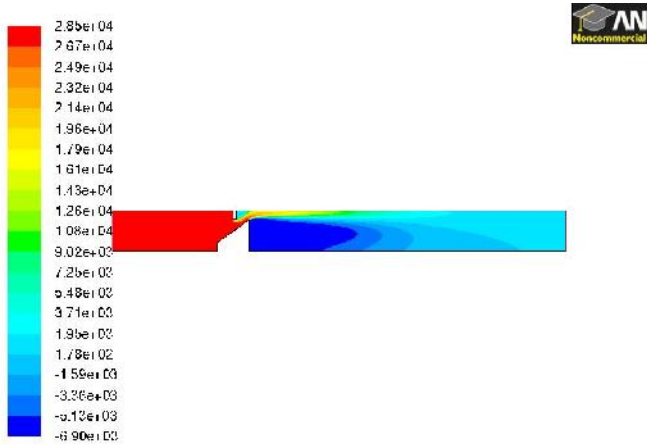


Figure 7. Total Pressure Contour for 5 l/s

The maximum total pressures are 18.3 kPa, 28.5 kPa and 72.9 kPa for the 4 l/s, 5 l/s and 8 l/s flows respectively. The minimum total pressure decreased with increase in volumetric flow rate in the flow field. With the 8 l/s flow rate having the least minimum total pressure of -17.8 kPa (see Table 2). The total pressure change in the flow fields for the 4 l/s, 5 l/s and 8 l/s are 22.70 kPa, 35.46 kPa and 90.7 kPa respectively. When compared to a mean operating pressure of 101.325 kPa, the aforementioned pressure changes represents 22.4%, 35% and 89.5% change.

Table 2. Maximum and Minimum Total Pressures in the Flow fields

Flow rates (l/s)	Maximum value (kPa)	Minimum value (kPa)	Maximum Change (kPa)	% change relative to the mean operating pressure
4	18.300	-4.400	22.700	22.4
5	28.500	-6.900	35.460	35.0
8	72.900	-17.800	90.700	89.5

Pressure Difference across Upper Plate

Total pressure is evaluated from the summation of static and dynamic pressure (Eq. 2). P_{0_1} , P_{0_2} are the total pressures at 25mm upstream and downstream respectively. Each is made up of the static (P) and dynamic pressures ($\frac{1}{2}\rho u^2$).

$$P_{0_1} = P_{0_2} + losses \quad (20)$$

A. 25mm upstream of bluff body condition

The total pressure profile for the different flow rates are shown on Fig.8. The total pressure for 8 l/s flow is the highest due to the fact that its flow velocity on this line is the highest (see Fig. 9). The total pressure is made up of static component mainly. The static pressure component of for the 4l/s , 5 l/s and 8 l/s flows constitutes 95.39%, 95.4% and 95.3% respectively. The maximum total pressure on at this line for the 4l/s, 5l/s and 8 l/s is shown on Table 3.

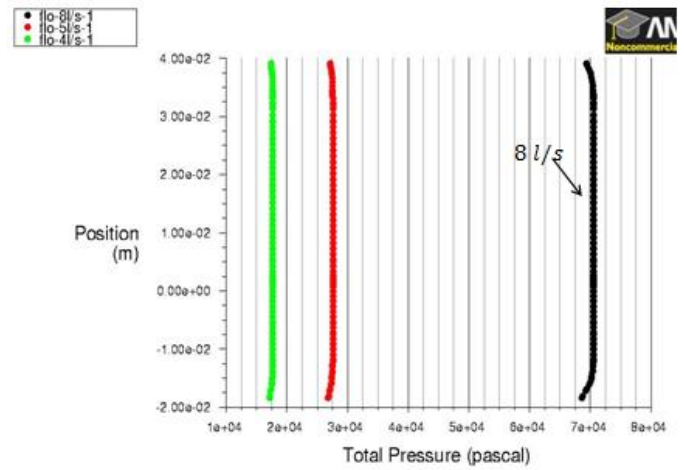


Figure 8. Total pressure 25mm upstream of upper plate

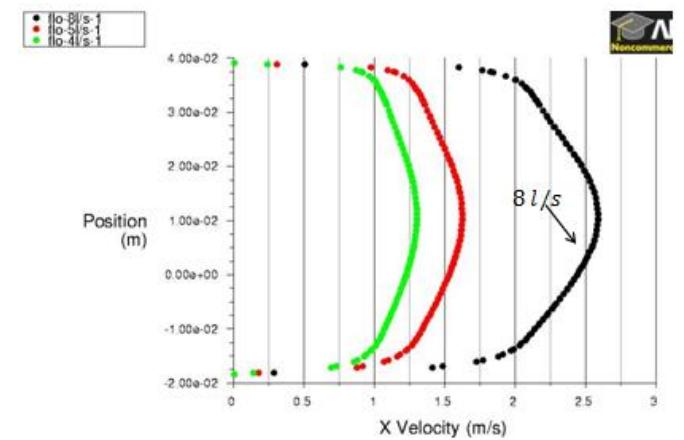


Figure 9. X-Velocity profiles at 25mm upstream of upper plate

Table 3. Total Pressure (Facet Average) change across upper plate

Flow rate (l/s)	Total Pressure (kPa)		Pressure Difference (kPa)
	25mm Upstream	25mm Downstream	
4	17.5936	0.2173	17.3763
5	27.4682	0.3241	27.1441
8	70.3758	0.7602	69.6156

B. 25mm downstream condition

The downstream condition for the three flows has two distinct regions – the stagnation and the turbulent region. The total pressures for the flows are shown in Fig. 10. They are made up of the static and dynamic components. *Stagnation region* ($-3.9 \times 10^{-2}m \leq y \leq 2.25 \times 10^{-2}m$): the total pressure (see Fig.10) is adverse (negative) pressure and is 100% static because x-velocity is zero (see Fig. 11). The turbulence intensity is slightly less than 25% (Fig. 12). *Turbulent region* ($2.25 \times 10^{-2}m \leq y \leq 3.9 \times 10^{-2}m$): This region experiences the highest velocity (see Fig. 11) and turbulence intensity (see Fig. 12). The total pressure her is main dynamic pressure (see Fig. 10 and 13). The Total pressure difference (using the fine mesh) 25mm upstream and downstream of the top plate for the three flows is shown on Table 3 With the 8l/s flow having the maximum total pressure change across the plate due to it's maximum turbulence intensity of over 250%

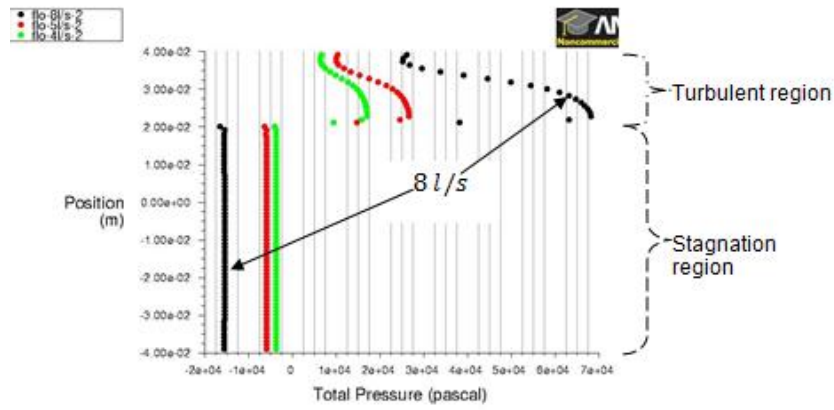


Figure 10. Total pressure 25mm downstream of upper plate

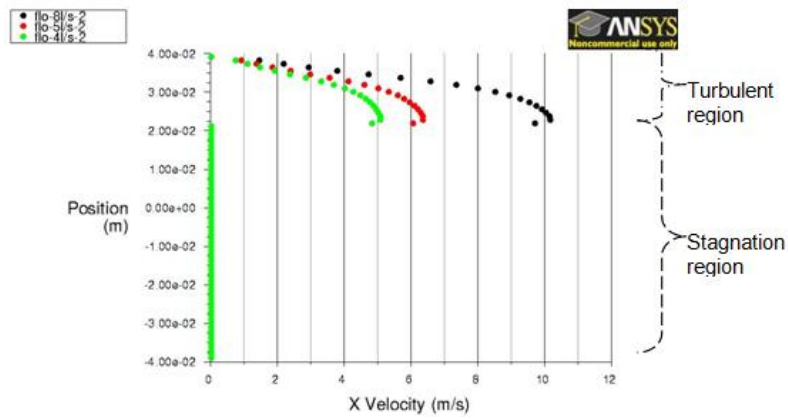


Figure 11. X - Velocity 25mm downstream of the upper plate

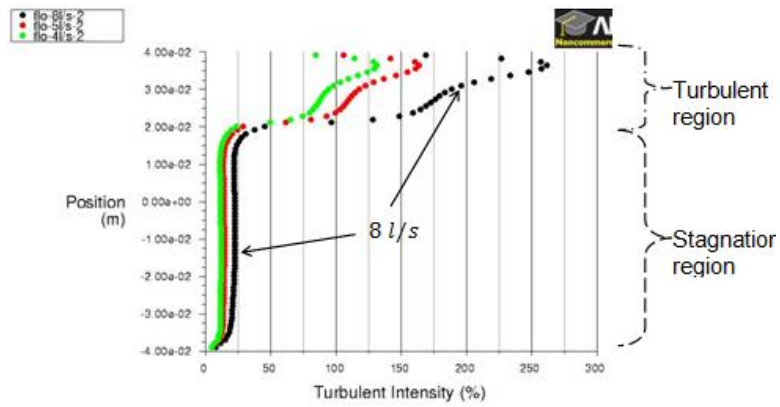


Figure 12. Turbulence intensity at 25mm downstream of upper plate

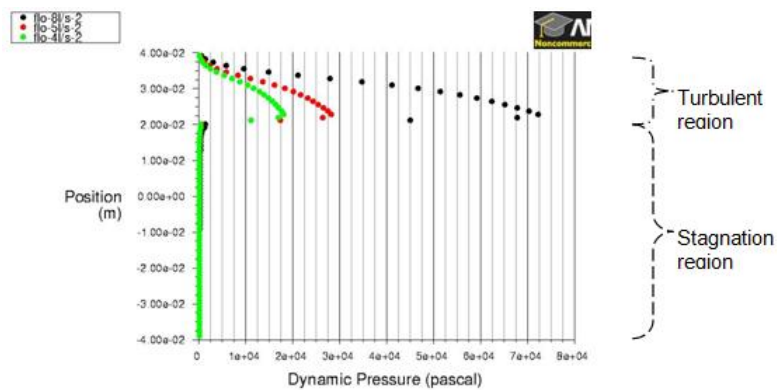


Figure 13. Dynamic pressures at 25mm downstream of the upper plate

(see Fig.12) exceeding those of the 4l/s and 5l/s flows which are ~130% and ~160% respectively. when compared with the mean operating pressure, the pressure difference represents 17.1% , 26.8% and 68.7% change for the 4 l/s , 5 l/s and 8 l/s flows respectively.

Pressure Difference across upper Plate (Course versus Fine Mesh)

The graphical representation of the total pressures 25mm upstream and downstream for the coarse and fine mesh used for the 5 l/s are shown on Fig. 14 and 15 respectively. The upstream section shows different profiles for the upstream pressures for the coarse and fine mesh (see Fig. 14). Table 4 shows the computed values for the total pressures for both meshes. The difference between the computed total pressure difference across the upper plate for the coarse and fine mesh is 0.464 kPa which represents 1.68 % increment over the fine mesh result. This implies that our solution for the coarse mesh is grid independent considering the fact that with ~299 % increase in number of cells from 13,580 cells (coarse grid) to 54,118 cells (fine grid), only 1.68% change was obtained in pressure difference. Within 1.68% error limit, the solutions from the coarse mesh could be relied on , hence the reduction in the computational cost of using the fine mesh.

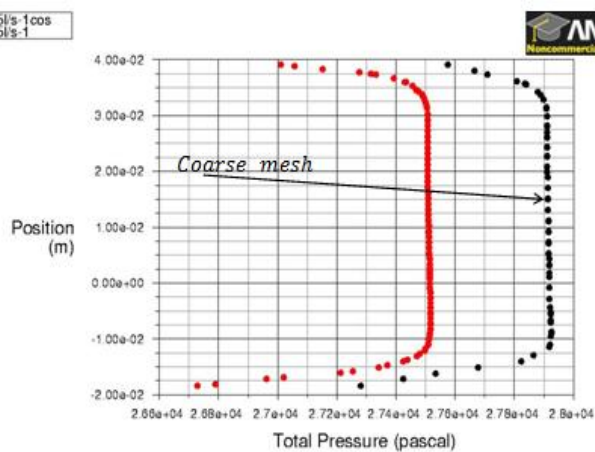


Figure 14. Total pressure 25mm upstream for Coarse and Fine mesh (5 l/s flow)

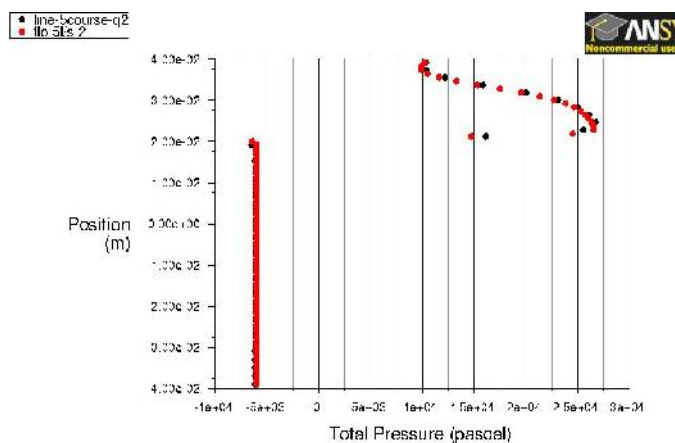


Figure 15. Total Pressure 25mm downstream for coarse and fine mesh (5 l/s flow)

Table 4. Total Pressure (Facet Average) 25mm upstream and downstream for 5 l/s Flow

Mesh	Total pressure (kPa)		Pressure Difference (kPa)
	25mm upstream	25mm downstream	
Fine	27.4681	0.3241	27.144
Coarse	27.8777	0.2697	27.608

Conclusion

The numerical experimentation carried out in this study, to simulate the flow of water in a variable area venturi meter using the commercially available CFD package Ansys fluent 12.0 version has shown that the pressure drop 25mm upstream and downstream of the upper plate is proportional to the volumetric flow rate across the plate. This proportionality is not linear. The total pressure drop across the plate for the 4 l/s, 5 l/s and 8 l/s flows are 17.38 kPa, 27.14 kPa and 69.62 kPa respectively. The losses in pressure across the plate are partly due to the level of turbulence (over 250%), which exceeds the values for the 4l/s and 5l/s flows which are ~130% and 160% respectively (see Fig. 12). When compared with the mean operating pressure (101.325 kPa), these pressure losses across the vertical plate represents 17.1%, 26.8% and 68.7% change for 4l/s and 5l/s flow situations. The difference between the computed total pressure difference for the coarse and fine mesh is 0.464 kPa. This represents 1.68 % increment over the fine mesh result. Within a reasonable error limit of 1.68% the results of the coarse mesh could be relied on, thus saving computational cost. Though results obtained in this work may not be relied on 100% because of the errors associated with the modelling, discretisation and iteration, it could serve as a good starting point for further study.

Nomenclatures

Symbol	Definition	Unit
A	Area	$[m^2]$
D	Pipe diameter	$[m]$
F	Force per unit mass	$[m/s^2]$
g	Acceleration due to gravity	$[m/s^2]$
I	Turbulence Intensity	$[\%]$
k	Turbulent kinetic energy	$[m^2/s^2]$
P	Static pressure	$[m^2]$
P_0	Total Pressure	$[N/m^2]$
ρ	Density	$[kg/m^3]$
t	Time	$[s]$
u	Velocity	$[m/s]$
ν	Kinematic viscosity	$[m^2/s]$
\dot{V}	Volumetric flow rate	$[m^3/s]$
x	Displacement	$[m]$
z	Elevation	$[m]$
μ	Dynamic viscosity	$[kg/ms]$
ν_T	Turbulent eddy viscosity	$[m^2/s]$
ϵ	Turbulent dissipation rate	$[m^2/s^3]$
σ_k	Turbulent kinetic energy Prandtl Number	$[-]$
σ_ϵ	Turbulent dissipation rate Prandtl number	$[-]$

Subscripts

1	upstream
2	downstream
i	x - direction
j	y -direction

Acknowledgement

The author wishes to specially appreciate Esso-Exploration and Production Nigeria Limited (EEPNL) for sponsoring my MSc programme at Cranfield University, UK where I got the opportunity to use the computational resources of the Applied Mathematics and Computing group, Cranfield University, UK for this research work.

REFERENCES

- Blazek, J. 2001. *Computational fluid dynamics: principles and applications*. Elsevier Science, Oxford.
- Chung, T. J. 2002. *Computational fluid dynamics*. Cambridge University Press, Cambridge.
- Durst, F. and Wang, A.B. 1989. Experimental and numerical investigation of the axisymmetric, turbulent pipe flow over a wall-mounted thin obstacle, *Seventh Symposium on Turbulent Shear Flows*, Stanford University, 21-23 August
- Fluent Inc. 2006a. *Fluent 6.3 user guide documentation*. Fluent Inc., Lebanon.
- Fluent Inc. 2006b. *Fluent 6.3 tutorial guide documentation*. Fluent Inc., Lebanon.
- Morris A. S. 2001. *Measurement and instrumentation principles*. Butterworth-Heinemann publishers, oxford.
- Patankar, S. V. and Spalding, D. B. 1972. A calculation procedure for heat, mass and momentum transfer in three-dimensional parabolic flows. *International J. Heat and Mass Transfer*, 15, 1787.
- Philip J, Sharma A., Jain N., and Nithin T. 2012. "Optimization of venturi flow meter model for the angle of divergence with minimal pressure drop by computational fluid dynamics method international conference on recent development in engineering and technology, 5th august, Mysore, ISBN-978-93-82208-00-6.
- Prajapati C. B., Patel V.K., Singh S.N. and Seshadri V. 2010. CFD analysis of permanent pressure loss for different types of flow meters in industrial applications: Proceedings of the 37th National and 4th International Conference on Fluid Mechanics and Fluid Power December 16-18, 2010, IIT Madras, Chennai, India.
